ISSN 1063-780X, Plasma Physics Reports, 2020, Vol. 46, No. 9, pp. 863–873. © Pleiades Publishing, Ltd., 2020.
Russian Text © The Author(s), 2020, published in Fizika Plazmy, 2020, Vol. 46, No. 9, pp. 771–782.

TOKAMAKS

Comparative Experiments on Lower Hybrid Wave Heating of Ions in High-Density Hydrogen and Deuterium Plasmas at the FT-2 Tokamak

S. I. Lashkul[a, *], A. B. Altukhov[a], A. D. Gurchenko[a], E. Z. Gusakov[a], V. V. D'yachenko[a], L. A. Esipov[a], V. A. Ivanov[a], O. A. Kaledina[a], M. Yu. Kantor[a], A. N. Konovalov[a], D. V. Kuprienko[a], M. I. Mironov[a], S. V. Shatalin[a], A. V. Sidorov[a], A. Yu. Stepanov[a], F. V. Chernyshev[a], and N. V. Tropin[a]

[a] *Ioffe Physical Technical Institute, St. Petersburg 194021 Russia*

**e-mail: Seguey.Lashkul@mail.ioffe.ru*

Received March 4, 2020; revised April 9, 2020; accepted April 20, 2020

Abstract—In the framework of the isotope effect studies at the FT-2 tokamak, the efficiencies were compared of the lower hybrid wave heating of the ion components of the hydrogen and deuterium plasmas with high densities (close to the Greenwald limit, $\langle n_e \rangle \leq 10^{20}$ m^{-3}). It was experimentally ascertained that, in accordance with the theoretical concepts, the efficient axial heating of the deuterium plasma ions occurs, as opposed to the peripheral heating of the hydrogen plasma ions. Such an isotope effect occurs due to the different localization of the plasma-RF wave interaction regions. The distinctive feature of these experiments is the fact that, in deuterium plasma, during the preliminary ohmic heating, the dependence of the energy lifetime on density $\tau_E(n)$ is linear (LOC dependence), and, with increasing density, the transition to the improved ohmic confinement mode occurs. In hydrogen plasma, on the contrary, the transition to the saturation mode is observed. In this study, the considerable decrease in τ_E was revealed, observed during the additional lower hybrid wave heating in both hydrogen and deuterium plasmas.

Keywords: RF ion heating, isotope effect, parametric instabilities, plasma diagnostics

DOI: 10.1134/S1063780X20090056

1. INTRODUCTION

Unfortunately, the large-scale studies of the plasma ion component heating using the RF waves of the lower hybrid (LH) frequency range (Lower Hybrid Heating, LHH), performed in the 1970s and 1980s, did not result in the development of the reliable heating technique. In most experiments performed at different tokamaks, the considerable ion heating was not obtained. One of the reasons for this is the development of the parametric decay instabilities (PDIs) at the discharge periphery at densities exceeding a certain threshold value, which is accompanied by the acceleration of ions [1]. Only in a few experiments performed at the JFT-2, Wega, Petula-B, and FT-2 facilities, an increase in the ion temperature was observed [1, 2]. Since then, the research on the interaction between the LH waves and the tokamak plasmas is focused on the drag current generation, which is efficient only at relatively low plasma densities. In this work, in the case of dense plasma, an attempt is made to revise the efficiency of the LH plasma heating with allowance for the characteristic features revealed during the isotope effect studies.

In the experiment at the FT-2 tokamak (a = 0.08 m, R = 0.55 m, 19 kA < I_{pl} < 34 kA, 2 T < B_T < 3 T, q_{95} ~ 3–6), the magnetron generator was used with a power of $P_{RF} \leq 200$ kW. The generator frequency (f_0 = 920 MHz) was close to the geometrical mean of the ion and electron cyclotron frequencies ($f_0 = (f_{ce}f_{ci})^{1/2}$) corresponding to a magnetic field of B_T = 2.2–2.5 T.

In this case, in the deuterium plasma (D-plasma), the LH resonance can be achieved only at the maximum attainable densities $\langle n_{e_res} \rangle \sim 1.2 \times 10^{20}$ m^{-3} [3, 4], which are close to the Greenwald limit $\langle n_{e_G} \rangle \sim 1.5 \times 10^{20}$ m^{-3} for I_{pl} = 30 kA. Thus, in the D-plasma, the linear interaction between the LH waves and the ion plasma component (stochastic heating) should occur in the axial region with the highest plasma density. In the hydrogen plasma (H-plasma), under the same conditions, the resonance densities are lower, $\langle n_{e_res} \rangle \sim 3.5 \times 10^{19}$ m^{-3}, and the interaction region is displaced towards the discharge periphery, namely, into the gradient region.

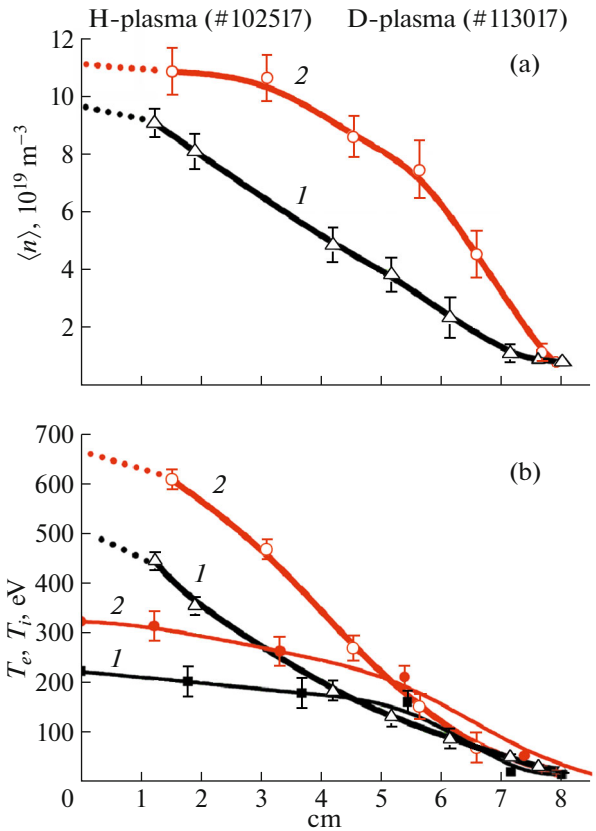

Fig. 1. Comparison between the profiles of basic plasma parameters for H-plasma (34.5 ms, black lines *1*) and D-plasma (35.5 ms, red lines *2*) in the OH high-density regime. (a) Density profiles and (b) electron and ion (two lower curves) temperature profiles.

Another important feature of the experiments described is the linear increase in the energy lifetime $\tau_E(\langle n_e \rangle)$ with increasing density (LOC mode), which is observed in the ohmic heating (OH) regime. In the D-plasma, this linear dependence is preserved up to densities of $\langle n_e \rangle \sim 7 \times 10^{19}$ m^{-3}, and with a further increase in density, the attributes of the transition to the improved ohmic confinement (iOC) regime are observed [5]. In the case of the H-plasma, the dependence $\tau_E(\langle n_e \rangle)$ becomes saturated (SOC mode) even at $\langle n_e \rangle \sim 5 \times 10^{19}$ m^{-3}.

In the high density regime (HDR, $\langle n_e \rangle \approx (0.8–1.2) \times 10^{20}$ m^{-3}), in the D-plasma, the total energy lifetime τ_E is of the order of 5 ms, which is approximately two times higher than that in the H-plasma under the same conditions [5]. In the HDR regime, at the same OH discharge scenario and the same initial parameters (B_T, I_{pl}), in deuterium (iOC regime), in contrast to hydrogen (SOC regime), the hotter plasma forms with the considerably wider density profile (Fig. 1). The formation of the steep density gradients at the plasma periphery accompanied by the observed sharp decrease in the D_β line intensity (in contrast to the behavior of the H_β line intensity in the H-plasma) [5] can be interpreted as the transition to the improved confinement regime with an external transport barrier (ETB). This fact makes the experiments on the lower hybrid ion heating in the high-density D-plasma even more relevant.

The article consists of Introduction, two sections and Appendix. In Section 2, the experimental scenario for the additional lower hybrid ion heating is presented and the characteristic details of the changes in the plasma energy balance are described. In the next section, the data obtained are analyzed and the main conclusions are drawn. In Appendix, the explanations are given necessary for understanding the peculiarities of using a number of diagnostics for measuring the high-density plasma parameters.

2. STUDIES OF ISOTOP EFFECT DURING LOW HYBRID ION HEATING IN HIGH-DENSITY REGIME

To measure the basic plasma parameters in the high-density regime (HDR), both standard and unique diagnostics were used, including the multipassage Thomson scattering diagnostics (TS), the enhanced scattering diagnostics (ES), the 2-mm-interferometer with seven channels (135–138 GHz), the five-channel scanning neutral particle analyzer (NPA), the soft X-ray diagnostics (SXR), the pyroelectric bolometer, and the movable Langmuir probes. Since, at high densities, it is difficult to measure a number of basic plasma parameters, the experimental data were analyzed and verified using the specially developed computer codes. Particular attention was paid to the possibility of measuring the density profiles $n_e(r, t)$ and the ion temperature profiles $T_i(r, t)$ (see Appendix).

2.1. Experimental Scenario

The additional LH heating of the hydrogen and deuterium plasmas was studied experimentally using the similar repeated HDR shots with the following parameters: $I_{pl} \sim 32–35$ kA, $\Delta t_{pl} \sim 60$ ms, $B_T \sim 2.4$ T, and $q_{95} \sim 3–3.5$ [5]. During the shots, the plasma density $\langle n_e(t) \rangle$ increased from $(4–5) \times 10^{19}$ to $(1–1.2) \times 10^{20}$ m^{-3} (Fig. 2). At the shot duration of $\Delta t_{pl} \sim 60$ ms, the duration of the stage with the quasi-stationary current I_{pl} was $\Delta t_{st} \sim 25$ ms. The RF energy pulse (f_0 = 920 MHz, and $P_{RF} \leq 150$ kW) with duration of $\Delta\tau_{RF} \sim 8–13$ ms was introduced at the 25–27th ms from the low field side of the toroidal magnetic field using the two-waveguide grill. The evolutions of the basic plasma parameters at the input powers of $P_{RF} = 70$ kW ($P_{in} = 42$ kW) for the D-plasma and $P_{RF} = 54$ kW ($P_{in} = 47$ kW) for the H-plasma are shown in Figs. 2a

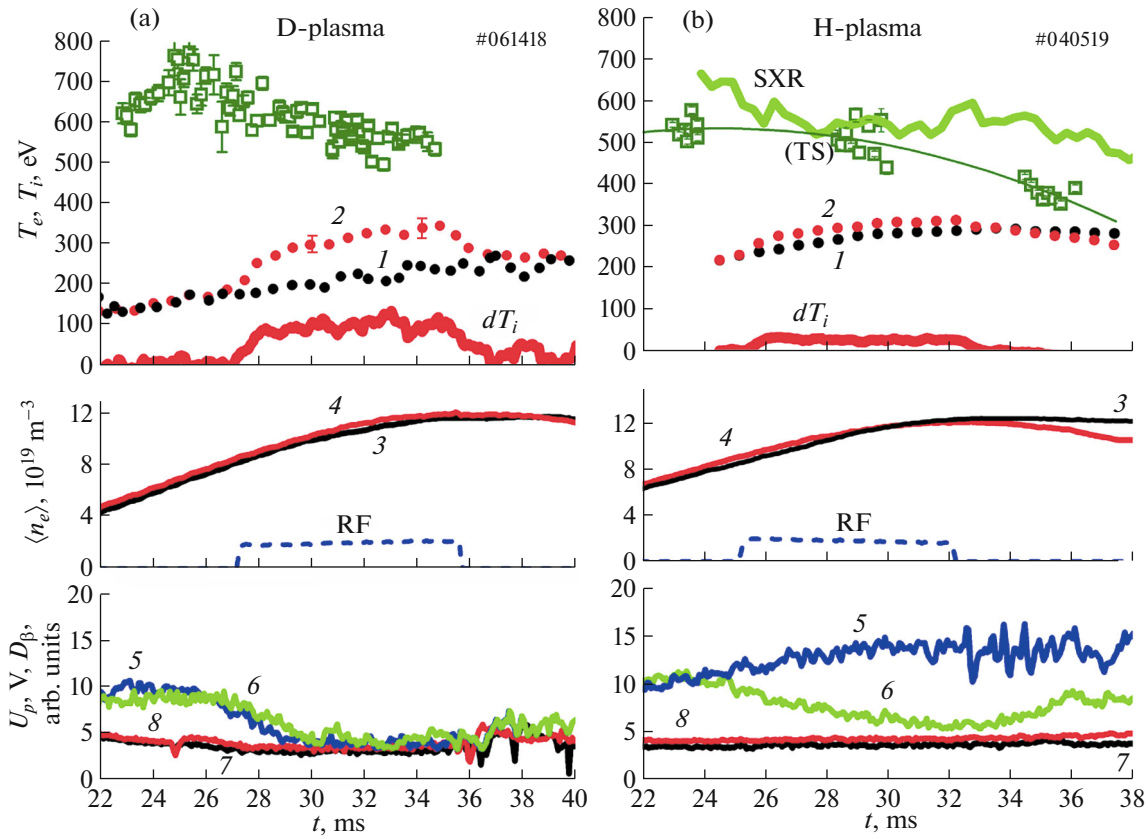

Fig. 2. (a) D-plasma parameters at $P_{RF} = 70$ kW ($P_{in} = P_{RF} - P_{ref} = 42$ kW) and (b) H-plasma parameters at $P_{RF} = 54$ kW ($P_{in} = P_{RF} - P_{ref} = 47$ kW). T_e is the central electron temperature measured by the TS (green squares) and SXR (green upper line in Fig. 2b) diagnostics; T_i is the ion temperature in the center of the plasma column (black dots *1* and red dots *2* correspond to the OH and LHH regimes); dT_i is the increment of the central ion temperature during the RF pulse relative to that in the OH regime (bold red lines); $\langle n_e \rangle$ are the mean densities in the OH (black lines *3*) and LHH (red lines *4*) regimes; H_β and D_β are the spectral line intensities (blue lines *5* and green lines *6* correspond to the OH and LHH regimes, respectively); and U_p is the loop voltage (thin black lines *7* and red lines *8* correspond to the OH and LHH regimes, respectively). The RF pulse duration is shown by the blue dashed line.

and 2b, respectively. The parameter $P_{in} = (P_{RF} - P_{ref})$, which is the difference between the direct and reflected RF powers, characterizes the power introduced into the tokamak chamber. In Fig. 2, the measured data for the D- and H-plasmas are compared to those for the OH shots. As can be seen from the data presented, despite some cooling of electrons, the additional heating of ions is observed both in the D- and H-plasmas. The temperature of the electron component was measured using both the TS laser diagnostics and the SXR diagnostics (see Fig. 2b). The comparison with the OH regime indicates that the additional RF heating has almost no effect on the increasing density dynamics $\langle n_e(0, t)\rangle$. As can be seen in Fig. 2, at the similar RF heating powers $P_{in} \approx 50$ kW, the considerably higher (three times) axial heating of the ion component occurs in the D-plasma, as compared to the H-plasma, that is the main manifestation of the isotope effect. Estimates performed using the ASTRA code show that, during the LHH, the total energy lifetime of the ion component

$$\tau_{E\,ion} = \int W_{ion} dV \Big/ \left[\int P_{ei} dV + P_{in} - \int (dW_{ion}/dt) dV\right]$$

decreases and becomes $\tau_{E\,LHH} \approx 0.75\tau_{E\,OH}$ and $\approx 0.85\tau_{E\,OH}$ for the D- and H-plasmas, respectively (Fig. 3). Here, P_{ei} is the power transported from electrons to ions. In this case, the heat loss associated with the charge exchange processes is not taken into account. In the OH regime, $P_{in} = 0$.

Such an isotope effect is observed at different input RF powers, as is shown in Figs. 4a and 4b using data of several experimental series. Here, we compare the increments of the axial ion temperature $dT_i(0, t)$ in the D- and H-plasmas, obtained when the input power P_{in} ranged from 20 to 110 kW. The axial ion heating in deuterium is several times higher than that in hydrogen. The characteristic features of the time evolution of the ion temperature profiles in the D-plasma ($P_{RF} =$

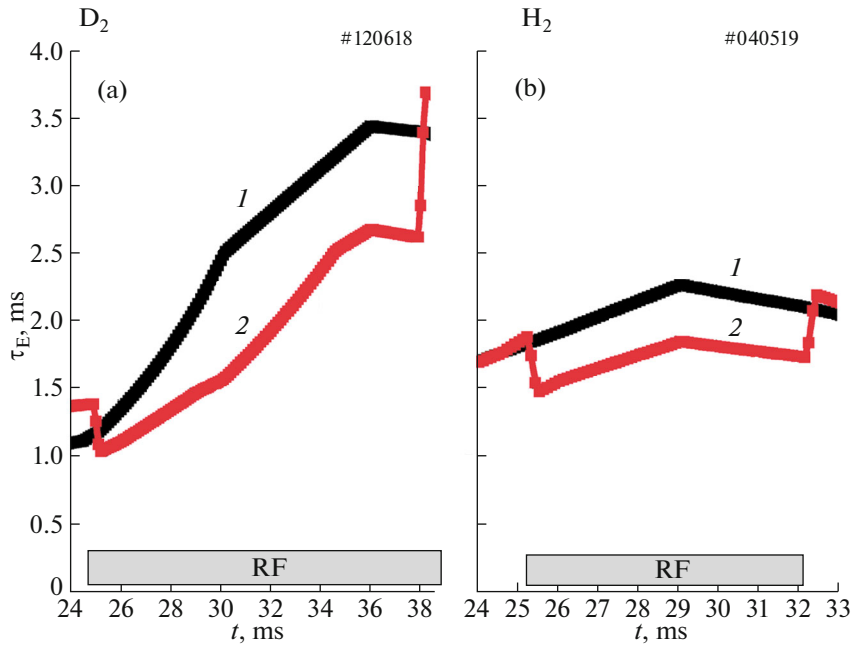

Fig. 3. Time evolution of τ_E in the regimes with increasing density (as in Fig. 2). Black lines *1* and red lines *2* correspond to the OH regime and the regime with the additional lower hybrid heating of the ion component, respectively. The dependences for the D- and H-plasmas were measured at P_{in} = 50 and 47 kW, respectively.

75 kW and P_{in} = 50 kW), as compared to those in the H-plasma (P_{RF} = 120 kW and P_{in} = 100 kW), are shown in Figs. 5a, 5b, and 6a, respectively. It can be seen that, despite the lower input power, the increment $dT_i(r)$ in deuterium is higher than that in hydrogen, for which it corresponds to the peripheral heating.

In deuterium, especially in the initial stage of the LH heating, the $dT_i(r)$ profiles have the peaked shape. In hydrogen, at low power P_{in} = 38 kW (Fig. 6b), the profiles are flattened and the increment $dT_i(r)$ increases towards the periphery. With increasing heating power (P_{in} = 100 kW), in the H-plasma, the small peak appears in the plasma center. As is known, during the LHH, the additional heating of the bulk of thermal plasma ions occurs due to thermalization of the high-energy "fast" ions that appear during the interaction between the RF wave and the thermal plasma ions [1]. Therefore, it is also convenient to diagnose the region of RF energy release (absorption) by means of recording the flow of the fast neutral charge exchange (CX) particles. As an example, in Fig. 7a, the spectra of the charge exchange atoms are compared, which were measured along the chord X = 4 cm in the H-plasma in both the OH regime (24.5 ms) and the additional LHH regime (27.7 ms). On the spectral dependence, at the 27.7th ms, a characteristic break is observed at a boundary energy of E_b ~ 1.3 keV, which illustrates the formation of the "tail" fast particles. The fact that, in the H- and D-plasmas, due to the isotope effect, the regions of the RF energy release (absorption) are different is confirmed by the normalized profiles of the fast neutral (FN) flows, shown in Fig. 7b for E_{CX} = 2600 eV. According to the model calculations [7] performed previously using the ASCOT code, the wide normalized profile of the FN flow (in the case of H-plasma) indicates that the RF power is released at the periphery. In contrast, in the D-plasma, the FN flow profile has the peaked shape, which corresponds to the axial heating.

2.2. Energy Balance of the Ion Component

At the equal parameters, in the D-plasma in the HDR with the extremely high densities, at a heating power of P_{RF} = 120 kW (P_{in} ≈ 110 kW), the considerable axial LH heating of ions was achieved (from $T_i^{OH}(0)$ = 300 eV to $T_i^{LHH}(0)$ = 450 eV), and an increase in temperature was $\Delta T_i^{LHH}(0)$ = 150 eV (see Fig. 4a). In the D-plasma, the efficiency of such heating is as follows:

$$\eta_{FT-2}^{D} = \frac{\Delta T_{ion}\bar{n}}{P_{RF}} = (8\text{–}12)\times 10^{13}\ \text{eV/kW cm}^3.$$

At the same time, in the H-plasma, the region of the RF power absorption is located closer to the periphery of the plasma column. At the similar input power P_{in} ≈ 100 kW, the heating of the H-plasma ions on the axis is considerably lower: from $T_i^{OH}(0)$ = 220 eV to $T_i^{LHH}(0)$ = 270 eV, that is, $\Delta T_i^{LHH}(0)$ = 50 eV.

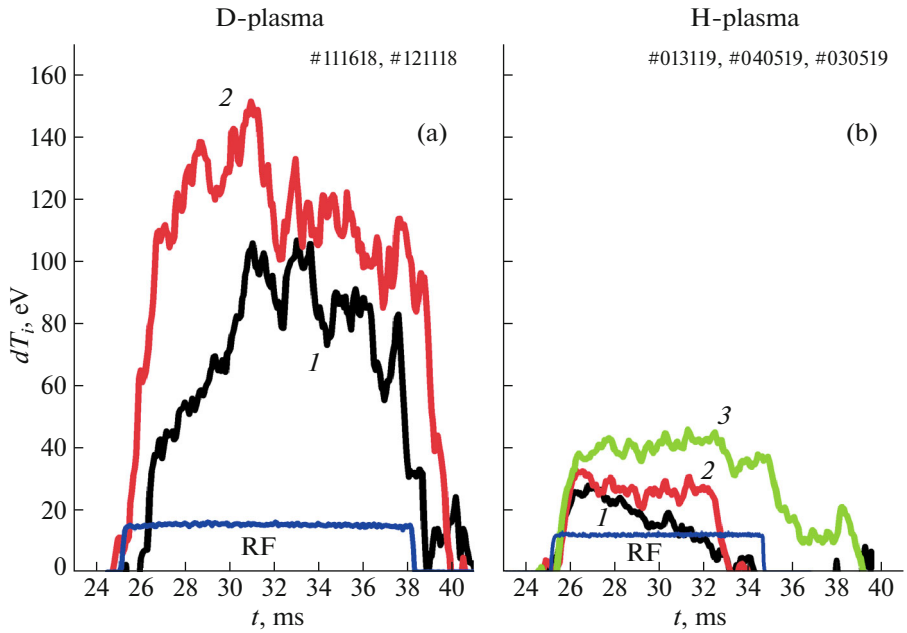

Fig. 4. Comparison of the increments of the central ion temperature $dT_i(0, t)$ at different input RF powers. (a) D-plasma: black line *1* and red line *2* correspond to $P_{in} = 20$ and 110 kW, respectively; (b) H-plasma: black line *1*, red line *2*, and green line *3* correspond to $P_{in} = 38$, 47 and 100 kW, respectively.

Of course, not all of the RF power entering the chamber P_{in} is spent on the additional heating of the thermal plasma ions. A certain part of it is lost on the diaphragm and the chamber walls, for example, due to the fast neutrals, which "have no time" for thermalization, and the parametric instabilities developing at the periphery of the plasma column. In addition, there may be other losses associated with the RF wave propagation inside the plasma column [1]. To accurately estimate the RF power P_{abs} absorbed by thermal ions, the model calculations are required of the energy balance of the ion component, which take into account the changes in the heat transport coefficients and cooling of ions in the charge exchange collisions with neutrals, which is beyond the scope of this article. The P_{abs} power (which is a part of the P_{in} power introduced into the chamber) can be roughly estimated by means of comparing the changes in the energy acquired by thermal ions $\Delta W_{ion\ LHH}$ during the LHH with the corresponding changes during the OH in the similar shots under assumption that, in the initial stage of the LHH, the ion energy lifetime does not change. According to Fig. 2, for the two discharges compared (OH and LHH), time evolutions of the electron density and temperature during the shot turned out to be identical. The only difference is that, during the additional LHH, the ion temperature and, accordingly, the ion energy content increase more intensively. Based on the definition of the energy lifetime $\tau_{E\ ion}$, it can be shown that $P_{abs} \approx \Delta W_{ion\ LHH}/\tau_{E\ ion}$. Powers that are received by the basal plasma ions from both electrons and RF wave (due to the Coulomb collisions between the "fast" ions and the thermal plasma ions) were calculated using the ASTRA code, based on the experimental data measured. As an illustration, for the H- and D-plasmas, the time evolutions of the ion component energy W_{ion} are shown in Figs. 8a and 8c. Here, the data are presented for both the OH shot and the OH shot with the additional LH heating, and, in the last case, the total energy content is $W_\Sigma = W_{ion\ OH} + \Delta W_{ion\ LHH}$. Based on these data, we can estimate the increment of the ion internal energy $\Delta W_{ion\ LHH}$ due to the LH heating. Considering the derivative $d\Delta W_{ion\ LHH}(t)/dt$ at times $t \approx \tau_{E\ ion}$, we can estimate the RF power transferred to the thermal ion component as $P_{abs} \approx d\Delta W_{ion\ LHH}(t)/dt \approx \Delta W_{ion\ LHH}/\tau_E$. As can be seen in Figs. 8b and 8d, in the initial stage of the additional heating after switching on the RF pulse, the fraction of power transported from the RF wave to deuterons is $P_{abs} = d\Delta W_{ion\ LHH}(t)/dt \sim (0.19–0.15)P_{in}$, while, for protons, it is $P_{abs} = \Delta W_{LHH}/dt \sim 0.22P_{in}$. The rest of power introduced into the chamber ($P_{in} - P_{abs}$) was lost on the diaphragm and the chamber wall, including the power loss due to the "fast" ions that "have not enough time" for thermalization.

The observed increase in the pyroelectric bolometer signal accompanied by the simultaneous decrease in the H_β line intensity (Fig. 9) can be considered as the evidence of such additional energy transport onto the wall. We note that we also did not observe the additional increase in the intensities of the emission

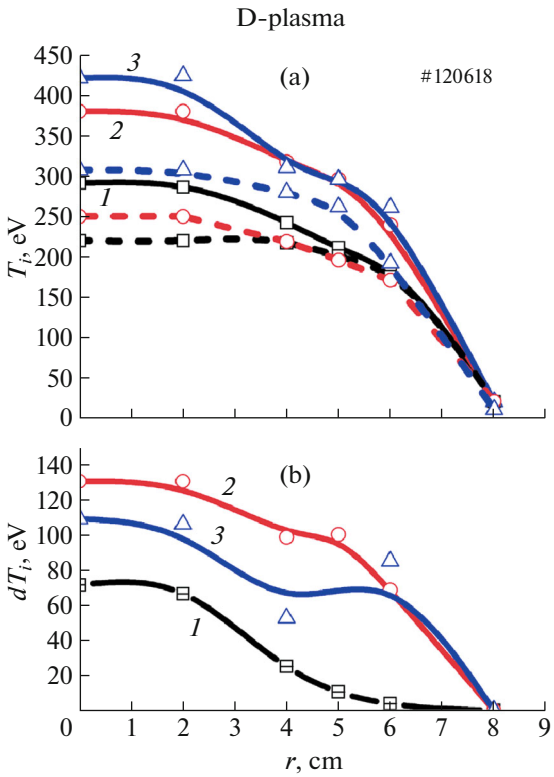

Fig. 5. (a) Time variation of the $T_i(r, t)$ profiles in D-plasma in the LHH regime (solid curves). The RF heating power is P_{RF} = 75 kW (P_{in} = 50 kW). The profiles measured at the 26th ms (squares and bold black line *1*), 29th ms (circles and red line *2*), and 38th ms (triangles and blue line *3*) are compared with the profiles measured in the OH regime at the same times (the same symbols, dashed lines). (b) Temperature increments $dT_i(r)$ (relative to the temperatures in the OH regime) measured at the 26 ms (black line *1*), 29 ms (red line *2*), and 38 ms (blue line *3*).

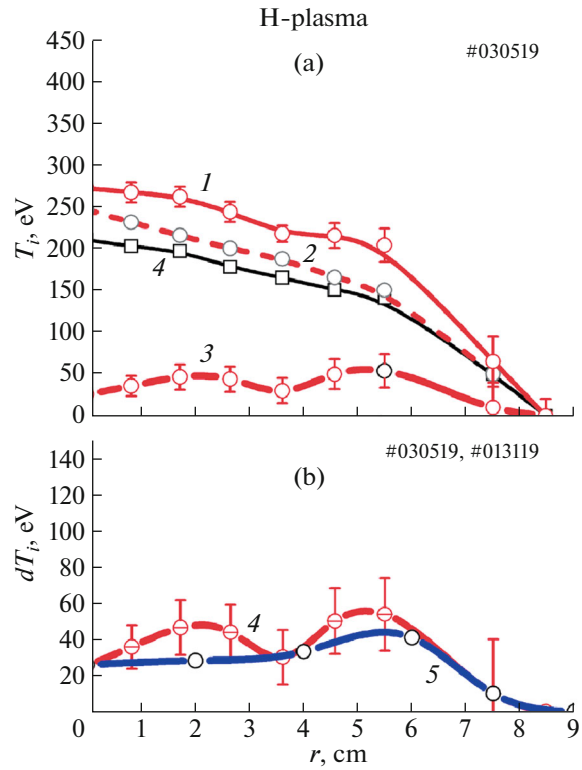

Fig. 6. (a) Comparison between the $T_i(r)$ profile obtained in the OH regime with the additional LHH (P_{RF} = 120 kW, P_{in} = 100 kW) in the H-plasma (red line *1*) and the profile measured at the same time in the OH regime with no additional heating (dashed red line *2*). Temperature increment $dT_i(r)$ (in the LHH regime relative to the OH regime) measured at the 27 ms is also presented (bold red line *3*). Squares and black line *4* correspond to the initial profile (the 24 ms) in the OH regime before switching on the additional LHH. (b) Comparison between the increments $dT_i(r)$ obtained at two RF powers in the H-plasma. Red line *4* and blue line *5* correspond to 100 and 38 kW of the RF power, respectively.

lines of light impurities and metal ions, corresponding to the first degrees of ionization. As for the hot ion emission from the axial regions, under conditions of the slight cooling of electrons and the equal increase in density (as compared to the OH regime), the additional contribution of hot ions to the P_{rad} bolometer signal during the LHH could hardly be expected. Therefore, the noted difference may occur due to the fact that the bolometer signal is determined by the total radiation flux P_{rad} coming from the plasma and consisting from both photons and atoms produced as a result of the charge exchange with the "fast" ions.

3. DISCUSSION AND CONCLUSIONS

The experimental data presented indicate that, in the high-density regime in the D-plasma with the additional LHH, the RF wave is absorbed in the axial region, as opposed to the peripheral absorption observed in the H-plasma. Such observations correspond to the theoretical concept [1] and the results of the model ray-tracing calculations for the pump wave presented in Fig. 10 and performed according to the technique described in [9]. As follows from Fig. 10, in the HDR in the D-plasma, at $\langle n_e \rangle = 10^{20}$ m^{-3} and a longitudinal deceleration of $N_{//} = 3$, the wave can reach the axial region, while, in the HDR in the H-plasma, it is absorbed at the periphery already at the beginning of the first turn of its trajectory. In the code used, the ray-tracing calculations were terminated, as soon as the point of the pump wave linear transformation was reached. The condition for the efficient RF energy absorption is the strong wave deceleration, when, for the wave number $k_\perp$, the following inequality is true: $\omega/(k_\perp v_{T_i}) < 2\sqrt{2}$ [1]. "Only ions with the perpendicular velocities $v_\perp$ higher than the phase velocity v_{ph} are subjected to the stochastic heating" [1]. In the region of the strong wave deceleration, only

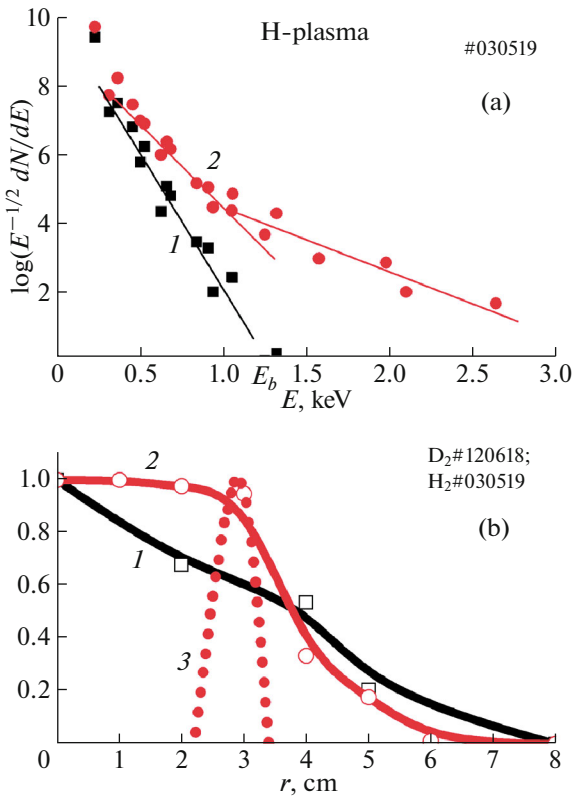

Fig. 7. (a) Comparison between the spectra of the charge exchange (CX) atoms in the H-plasma. The CX atom flows are presented measured along the chord $X = 4$ cm in the OH regime (24.5 ms, black squares and line *1*) and in the OH+LHH regime (27.7 ms, red circles and line *2*). P_{RF} = 120 kW (P_{in} = 100 kW). E_b is the energy corresponding to the lower boundary of the high-energy "tail" of the CX atom energy distribution. (b) Comparison between the normalized chord profiles of the fast neutral (FN) flows at E_{CX} = 2.6 keV. Black line *1* and red line *2* correspond to the D- and H-plasmas, respectively. For the H-plasma, the inverse FN radial profile is additionally presented (red dots *3*).

the ions from the "tail" of the Maxwellian distribution, with energies $E_i > (6–8)T_i$, were accelerated [2]. The conditions for the LH heating are determined by the ratio of the thermal velocity of ions to the minimum transverse phase velocity of the wave: $\delta_i = v_{ph\perp min}/v_{T_i} \approx (2E_b/T_i)^{1/2}$, where E_b is the limiting energy of the accelerated ions (see Fig. 7a). According to the experimental data obtained at other facilities and results of numerical calculations, the considerable heating was obtained at $\delta < 3.5–4$ (Fig. 4.11 in [1]). In our case, based on the data shown as an example in Fig. 7a, where $E_b \approx 1.2$ keV and $T_i = 200$ eV, in the HDR in the H-plasma, we can make the following estimate: $\delta_i \leq 3.5$. In the HDR in the D-plasma, we obtain $\delta_i \leq 3.2$, which agrees with the above estimates.

The heating of the bulk of plasma ions occurs as a result of collisions with the high-energy ions. The efficiency of such stochastic heating depends on the plasma density and the lifetime of fast ions, which can be lost due to, for example, the mechanism of orbit loss [7] and the charge exchange processes. Moreover, the efficiency is also determined by the parametric decay instability (PDI), which develops in the outer discharge region and causes the strong peripheral absorption. It is known that the PDI intensity increases with increasing density and plasma cooling at the periphery [10]. As a result, the heating efficiency decreases. We note that, in the experiments described, when the density increased during the shot, and the transition to the HDR occurred, after the predictable increase in the instability intensity, the considerable PDI suppression was observed in both hydrogen and deuterium [11]. The possible reason for this phenomenon is an increase in the collision rates at the discharge periphery, which, of itself, can result in the PDI suppression [12]. The phenomena associated with the PDI development and suppression, occurring as a result of interaction between the LH wave and plasma, have been studied for a long time at the FT-2 facility [2, 13].

Thus, the main results of this study are as follows.

(1) It has been experimentally confirmed that, in accordance with the theoretical concepts, in the HDR operating regime, the efficient axial heating of ions is observed in the D-plasma (Figs. 5 and 6), as opposed to the peripheral heating observed in the H-plasma in the same operating regime. This isotope effect occurs due to the different localization of the interaction regions in the plasma volume. In experiment with the additional lower hybrid heating (P_{in} ~ 110 kW), the axial temperature of deuterons increases by 150 eV, as compared to the OH regime (from 300 to ~ 450 eV, Fig. 4), which corresponds to the unbeatably high heating efficiency $\eta^{D}_{FT-2} = (8–12)\times10^{13}$ eV/kW cm^3.

(2) In the HDR with the additional lower hybrid ion heating, the considerable decrease (by approximately 20%) in the plasma energy lifetime is observed. In the D-plasma, $\tau_E^{LHH} \approx 0.75\tau_E^{OH}$; in the H-plasma, the decrease in the energy lifetime is less pronounced, $\tau_E^{LHH} \approx 0.85\tau_E^{OH}$. At the same time, in the D-plasma, the τ_E^{LHH} absolute value remains considerably higher than that in the H-plasma, i.e., $\tau_E^{LHH} \approx 2.7$ ms and $\tau_E^{LHH} \approx 1.7$ ms, respectively (Fig. 3).

(3) Under assumption that, in the initial stage of the additional heating, the energy lifetime is the same as in the OH stage, it is possible to estimate the fraction of the RF power absorbed by thermal ions. In the H-plasma, it turns out to be higher than that in the D-plasma: $P^{H}_{abs} \approx 0.22P_{in}$ and $P^{D}_{abs} \approx (0.19–0.15)P_{in}$, respectively (Fig. 8).

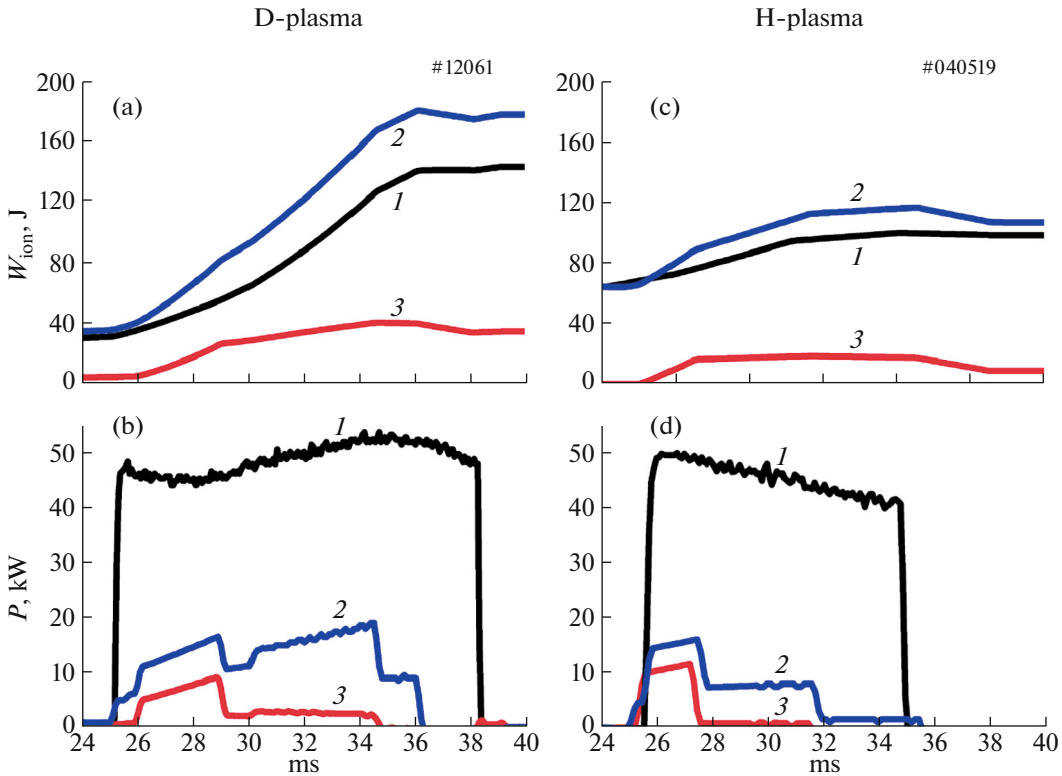

Fig. 8. (a) and (c) Comparison between the time evolutions of the energy content of the ion component W_{ion} of the D/H-plasmas in the OH (black lines *1*) and OH + LHH ($W_\Sigma = W_{OH} + \Delta W_{LHH}$, blue lines *2*) regimes with increasing density (see Fig. 2). Red lines *3* correspond to the energy content increment ΔW_{LH} of the ion component obtained only due to the LHH. (b) and (d) Comparison between powers: P_{in} is power inputted into the chamber (black lines *1*); $P_{abs} = dW_\Sigma/dt$ is the total power absorbed by the basic plasma ions due to both the ion–electron collisions and the interaction with the LH wave (blue lines *2*); and $d\Delta W_{LHH}/dt$ is the fraction of power absorbed by ions only due to the interaction with the LH wave (red lines *3*).

Thus, in the high-density deuterium plasma, the efficient axial heating of ions occurs, while, in the H-plasma, the RF energy is efficiently transported to the entire plasma. One of the reasons for this may be related to the better confinement of fast suprathermal protons generated by the LH wave due to the fact that the width of their "banana" orbits ($\delta \sim m_i^{-1/2}$) is less than that for deuterons. In addition, at the same energies, the velocity of "suprathermal" protons is $\sim(m_d/m_p)^{1/2}$ times higher. Therefore, the wave energy can be more efficiently transported to the "tail" ions in the Maxwellian distribution of protons. Subsequently, the bulk of ions are heated due to collisions with these suprathermal ions.

In this paper, we do not consider the phenomena related to the changes in the confinement mechanism occurring when the RF power is introduced into plasma. This will be the subject of further research. In particular, we plan to study the heat transport conditions in the HDR regime, including those at the periphery of the D- and H-plasmas and in the SOL in both the OH regimes and the OH regimes with the additional LHH.

APPENDIX

DISTINCTIVE FEATURES OF MEASURING AND MODELING THE DISCHARGE PARAMETERS AT HIGH DENSITIES

A. The complex approach was used to reconstruct the density profiles, which included both the local Thomson scattering (TS) measurements along the vertical chord shifted 1.5 cm from the center and the integrated phase measurements performed with the help of the microwave interferometer with seven vertical sounding chords.

During the interferometry measurements, the plasma was probed using the ordinary wave with a frequency of $f_i = 135–138$ GHz. The dependence of the measures phase shift on the plasma density is as follows:

$$\Delta\Phi(t) = \frac{2\pi L}{\lambda}\left(1 - \left(1 - n_e(t)/n_c\right)^{1/2}\right), \qquad (A.1)$$

where L is the path length in the plasma, λ is the wavelength of the probe radiation, and $n_c = m_e\pi f_i^2/e^2$ is the critical density [6]. The distinctive feature of the inter-

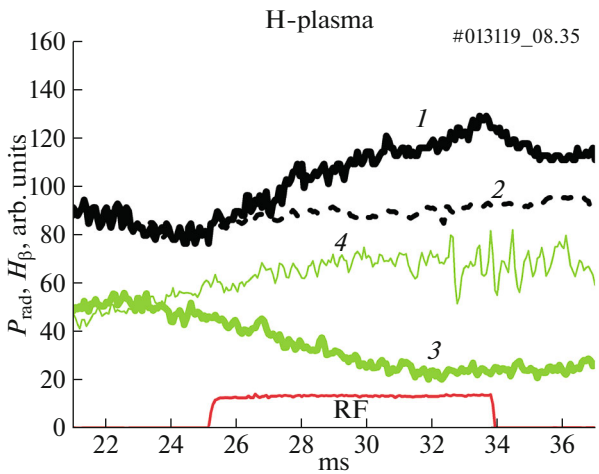

Fig. 9. Comparison between the time variations of the bolometer signals along the central chord: P_{rad}^{LHH} (solid black line *1*) and P_{rad}^{OH} (dashed line *2*). Green curves *3* and *4* correspond to the H_{β_LHH} line intensity in the LHH experiment and the H_{β_OH} line intensity in the OH experiment, respectively. Red line shows the RF pulse duration.

ferometry measurements in the high-density plasma is the strong refraction of the probe beam. The ray trajectories became curved, so the dependence of the phase shift on the density turns out to be nonlinear that, along with an increase in the path travelled, additionally contributes to the measured phase difference [6]. In the expression relating the electron density to the experimentally measured phase,

$$n(t) = n_c\left(\frac{\Phi(t)\lambda}{\pi L} - \left(\frac{\Phi(t)\lambda}{2\pi L}\right)^2\right), \qquad \text{(A.2)}$$

the quadratic term becomes important. The procedure for reconstructing the density profile using data of the chord measurements consists in the sequential accumulation (from the base to the apex) of the cylindrical layers of equal density. In the case of the straight rays, in the linear approximation, the density, radius, and horizontal shift of each layer are chosen using the condition that the phases at the layer edges coincide with those on the approximating profile. In the case of the curved rays, in expression (2), the quadratic term must be taken into account. In addition, the analytical calculations of the ray trajectory between the probing and receiving horn antennas are required. Since, under conditions of the strong refraction, the maximum signal power may correspond not to the central ray, the next step in processing the measurement results is the ray tracing calculations in the geometrical optics approximation. In these calculations, the density profile obtained in the first stage is used, and the real antenna patterns are taken into account. Then, the integrated phase is calculated for a given set of rays. The density profile is reconstructed as a result of the iterative procedure, during which the experimentally measured phases are compared with the calculated ones. In calculations, the rays forming the beam are considered separately, and the diffraction effects are not taken into account. This procedure considerably increases the reliability of the radial density profile reconstruction.

The interferometry measurements were used to calibrate the relative densities obtained using the local Thomson scattering diagnostics. The calibration was performed by means of correlating the Thomson scattering data with the integrated density measured by the interferometer along the vertical chord coinciding with the axis of the laser sounding. Moreover, to increase the reliability, the absolute calibration of the density profile measured using the TS diagnostics was usually performed in the initial discharge stage at the relatively low electron densities, when the refraction effects are small.

B. The ion temperature profiles $T_i(r)$ were measured using the five-channel nuclear particle analyzer (NPA) [14], which can scan the plasma from shot to shot in the vertical plane. The ion temperature was determined by means of analyzing the recorded energy distributions. Under conditions of the FT-2 tokamak, the applicability of this method was confirmed by the

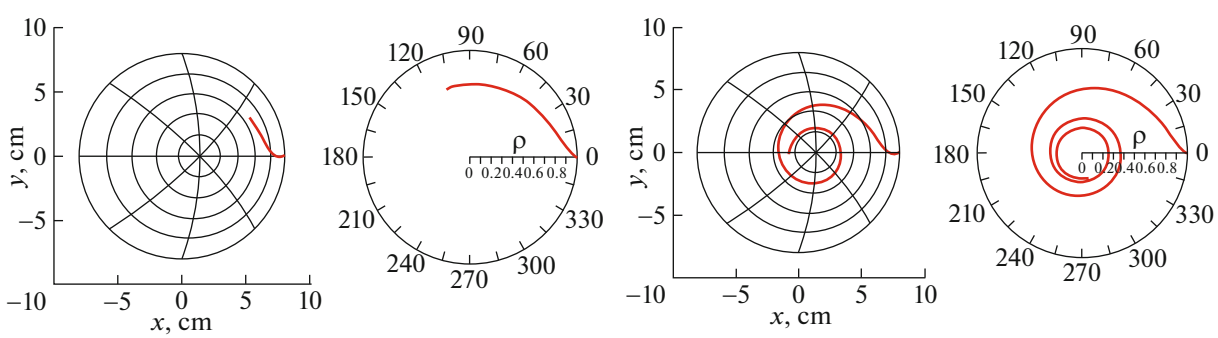

Fig. 10. The pump wave trajectory in projections onto the poloidal and toroidal tokamak sections for the H/D plasmas. Here, $\rho = (R - R_{inner})/(R_{outer} - R_{inner})$, where R is the distance between the inside and outside of the torus counted from the torus major axis in the equatorial plane. The used parameters are: $\langle n_e \rangle = 10^{20}$ m^{-3} and $N_{//} = 3$.

calculations using the ASCOT code [7]. As a result, it was shown that the direct determination of the ion temperature is possible in the plasma density range of $\langle n_e \rangle \leq (4–5) \times 10^{19}$ m^{-3}. Using the calculations, it is also possible to determine the region of the RF power direct absorption from data on the source localization of the high-energy charge exchange atoms with energies $E_{CX} \geq 2$ keV. In the denser plasma with $\langle n_e \rangle \geq (5–6) \times 10^{19}$ m^{-3}, the flow of charge exchange atoms from the axial region of the plasma column decreases when it passes through the peripheral plasma layers. This effect is important, since it complicates the direct measurements of the $T_i(r)$ profile. Therefore, to correct the ion temperatures determined from data on the NPA measurements, the model calculations were additionally performed using the DOUBLE-MC Monte Carlo code, which involve the entire experimental data array [8]. To simulate the charge exchange atom flow along the observation line, the following integral expression is considered:

$$\Gamma_0(E) = \int_0^L n_i(x) \sum_j \left[n_j^0(x) \left\langle \sigma_j^0 v \right\rangle_{v_j} \right] f_i(E,x) \mu(E,x) dx, \quad (A.3)$$

where E is the energy of particles (the plasma atoms and corresponding ions escaping from the plasma); $n_i(x)$ is the ion density of the basic plasma; $n_j^0(x)$ is the density of donors of the j type contributing to the neutralization process; $\langle \sigma_j^0 v \rangle_{vj}$ is the corresponding reaction rate averaged over the distribution of the relative velocity of ions and donors; $f_i(E, x)$ is the ion energy distribution function; $\mu(E, x)$ is the factor characterizing the atom flow loss due to the processes resulting in their repeated ionization; and x is the coordinate along the observation line. Summation is performed over the basic processes resulting in the neutralization of plasma ions. For the FT-2 tokamak, the most significant are the charge exchange processes between the ions and plasma neutrals, as well as the radiation recombination of ions and electrons. The integration is performed along the chord, the length L of which is determined by the intersections of the observation line with the boundaries of the poloidal section of the plasma volume. The $f_i(E)$ ion energy distribution function is set to be the Maxwellian function, and the density and temperature profiles of ions and electrons are assumed to be the double parabolic functions approximating the experimental data. The expression for the atom flow loss factor has the following form:

$$\mu(E,x) = \exp\left\{ -\int_x^L \sum_k \left[n_k^i(l) \frac{\left\langle \sigma_k^i v \right\rangle_{v_k}}{v} \right] dl \right\}, \quad (A.4)$$

where $n_k^i(l)$ is the density of the corresponding plasma component that contributes to the process k resulting in the ionization; $\langle \sigma_k^i v \rangle_{vk}$ is the reaction rate averaged over the distribution of the relative velocity of the emitted atoms and the plasma component k; v is the velocity of particles (the plasma atoms and corresponding ions escaping from the plasma); and l is the coordinate along the observation line. Summation is performed over the basic processes contributing to the ionization of atoms escaping from the plasma center. In the case of the FT-2 tokamak, the most significant processes are the charge exchange processes between the ions and plasma neutrals, as well as the ionizations by the electron and ion impact.

The upper boundary of the energy range, used in determining the ion temperature in the OH regime, was limited to 1.6 keV. This is due to a decrease in the signals of the NPA detection channels to the noise level, which occurs with increasing energy, which, in turn, can be explained by the exponential decay of the ion energy distribution function at high energies. Since, at low energies, the loss factor (3) is rather high, the energy flows come to the NPA mainly from the peripheral plasma regions, where the ion temperature is lower than in the axial region. As a result, for the chosen energy range $E_{CX} \leq 1.6$ keV, the measured ion temperatures $T_{\text{ion, eff}}$ turn out to be considerably lower than the true temperatures T_{ion}, which was demonstrated by the model calculations using the DOUBLE-MC code. The calculations were used to correct the temperature estimate by means of introducing the correction coefficients $K = T_{\text{ion, eff}}/T_{\text{ion}}$. The coefficients were determined by means of comparing the set and calculated profiles $T_{\text{ion}}(r)$. The obtained dependence of the correction coefficients $K(n, x)$ on the density were used to make the scaling corrections to the experimental temperatures $T_{\text{ion, eff}}(r, t)$ measured in the axial region $0 \leq r \leq 3.5$ cm. As an example, for the D- and H-plasmas, the coefficients $K(n, x)$ calculated for the central chord of the plasma section, $x = 0$, are shown in Fig. 11.

The modeling using the DOUBLE_MC code was performed in two stages. In the first stage, the neutralization target was calculated, i.e., the density of all donors involved in the neutralization. Using the Monte Carlo method, the penetration of neutral particles through the peripheral plasma was calculated. Next, the target was calculated, which formed as a result of the recombination processes. To do this, we used the equations of the ionization balance in the approximation of the corona equilibrium. In the second stage, the energy distribution of the escaping atoms was calculated in accordance with expression (2). We also performed calculations of the auxiliary parameters, such as, for example, the luminosity function characterizing the probability of production of atom with a certain energy in a given point of the plasma and its further escape from this point. Thus, the use of the DOUBLE-MC code made it possible to establish the correspondence between the energy distributions of

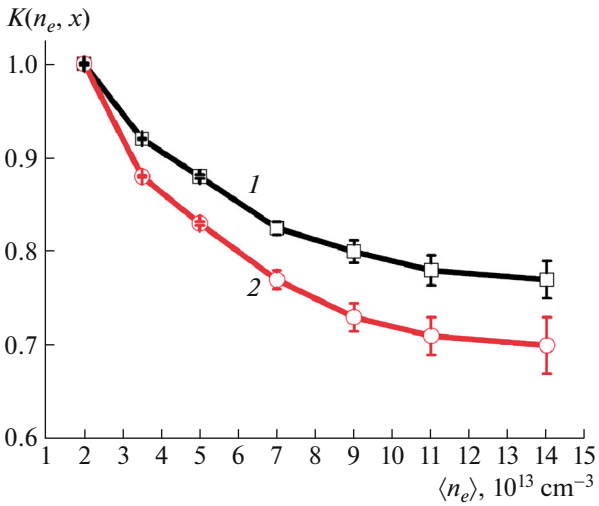

Fig. 11. Correction coefficients $K(n, x)$ for the central chord of the plasma cross section calculated under assumption that the edge temperature of the working gas is T_{ew} = 3–5 eV. Curves *1* and *2* correspond to the H- and D-plasmas, respectively.

atoms escaping from the plasma and plasma ions. By means of varying the ion temperature used in the simulations, we can establish the correspondence between the calculated and experimental energy distributions of the escaping atoms. At densities of $\langle n_e \rangle \leq (4–5) \times 10^{19}$ m^{-3}, the simulations performed in accordance with the above scenario made it possible to directly determine the ion temperatures over the entire plasma section, and at high densities (in the HDR regime), it was possible only in the radial range of 3.5 cm $\leq r \leq$ 8 cm, where a decrease in the charge exchange atom flow from the axial regions is not important.

In the axial regions of the plasma column, the profiles were corrected using the correction coefficients $K(n, x)$.

Thus, in the HDR regime, under conditions of the plasma density increasing with time, it was necessary to correct the ion temperature measured in the axial regions. The correction was performed using the coefficients $K(n, x)$ in both the OH regime and the LHH regime, when, as a result of interaction between the RF wave and the plasma, the high-energy particles ($E_{CX} \geq$ 2 keV) appeared in the energy distribution of ions.

We also note that the technique for determining the ion temperature profiles form data on the charge exchange atom flows can be sensitive to the effects of the magnetic field rippling, which consist in the loss of the so-called locally trapped ions. Indeed, at the FT-2 facility, the magnetic field rippling is rather high (10% in the limiter region). However, as the simulations using the ASCOT code [7] show, at the FT-2 tokamak, the loss of the locally trapped ions is negligible. This is due to the strong poloidal rotation of the plasma resulting in the considerable changes in the ion drift orbits. As a result, the effect of the magnetic field rippling on the ion temperature measurements can be neglected.

FUNDING

The studies of the isotope effect were supported by the Russian Scientific Foundation (project no. 1712-01110). The operation of the FT-2 tokamak and its standard diagnostic systems was supported by Ioffe Institute under the State Contract no. 0040-2014-0023.

REFERENCES

1. V. E. Golant and V. I. Fedorov, *Methods of High-Frequency Plasma Heating in Toroidal Fusion Devices* (Energoizdat, Moscow, 1986), pp. 69–96, 116–141 [in Russian].
2. V. N. Budnikov and M. A. Irzak, Plasma Phys. Controlled Fusion **38**, A135 (1996).
3. S. I. Lashkul, A. B. Altukhov, A. D. Gurchenko, E. Z. Gusakov, V. V. Dyachenko, L. A. Esipov, M. A. Irzak, M. Yu. Kantor, D. V. Kouprienko, A. A. Perevalov, A. N. Saveliev, S. V. Shatalin, and A. Yu. Stepanov, Nucl. Fusion **55**, 073019 (2015).
4. S. I. Lashkul, A. B. Altukhov, A. D. Gurchenko, E. Z. Gusakov, V. V. Dyachenko, L. A. Esipov, M. A. Irzak, M. Yu. Kantor, D. V. Kouprienko, A. N. Saveliev, A. Yu. Stepanov, and S. V. Shatalin, Plasma Phys. Rep. **41**, 990 (2015).
5. D. V. Kouprienko, A. B. Altukhov, A. D. Gurchenko, E. Z. Gusakov, L. A. Esipov, O. A. Kaledina, N. V. Tropin, S. I. Lashkul, G. A. Troshin, and S. V. Shatalin, Plasma Phys. Rep. **45**, 1128 (2019).
6. V. E. Golant, *Microwave Plasma Diagnostics* (Nauka, Moscow, 1968) [in Russian].
7. T. Kurki-Suonio, S. I. Lashkul, and J. A. Heikkinen, Plasma Phys. Controlled Fusion **44**, 301 (2002).
8. M. I. Mironov, Candidate's Dissertation in Physics and Mathematics (Ioffe Institute, St. Petersburg, 2010).
9. Yu. F. Baranov and V. I. Fedorov, Nucl. Fusion **20**, 1111 (1980).
10. R. Cesario, L. Amicucci, A. Cardinali, C. Castaldo, M. Marinucci, F. Napoli, F. Paoletti, D. De Arcangelis, M. Ferrari, A. Galli, G. Gallo, E. Pullara, G. Schettiniand, and A. A. Tuccillo, Nucl. Fusion **54**, 043002 (2014).
11. S. I. Lashkul, A. Yu. Stepanov, A. B. Altukhov, A. D. Gurchenko, E. Z. Gusakov, V. V. Dyachenko, L. A. Esipov, M. A. Irzak, M. Yu. Kantor, and D. V. Kouprienko, EPJ Web Conf. **149**, 03012 (2017).
12. C. Castaldo, A. Di Siena, R. Fedele, F. Napoli, L. Amicucci, R. Cesario, and G. Schettini, Nucl. Fusion **56**, 016003 (2016).
13. V. V. D'yachenko, A. N. Konovalov, A. Yu. Stepanov, A. B. Altukhov, E. Z. Gusakov, L. A. Esipov, S. I. Lashkul, and S. V. Shatalin, Plasma Phys. Rep. **45**, 1134 (2019).
14. V. V. Afrosimov, E. L. Berezovskii, I. P. Gladkovskii, A. I. Kislyakov, M. P. Petrov, and V. A. Sadovnikov, Sov. Phys. Tech. Phys. **20**, 33 (1975).

Translated by I. Grishina